Automated algorithm to detect changes in geostationary satellite's configuration and cross-tagging

Phan Dao

Air Force Research Laboratory
Space Vehicles Directorate
Kirtland AFB, Albuquerque, NM 87117

ABSTRACT

Using broadband and color photometry, analysts can evaluate satellite operational status and affirm its identity. The process of ingesting photometry data and deriving satellite physical characteristics can be undertaken by analysts in batch mode, meaning using an entire batch of data at the conclusion of each observation night, or by automated algorithms in a batch or on-line mode of operation. In an on-line mode, the assessment is generated with each new data point. Tools used for detecting change to satellite's status or identity, whether performed with a human in the loop or automated algorithms, are generally not built to detect with minimum latency and traceable confidence intervals. To alleviate those deficiencies, we investigate the use of Hidden Markov Models (HMM), in a Bayesian Network framework, to infer the hidden state (changed or unchanged) of a three-axis stabilized geostationary satellite using broadband and color photometry. Unlike frequentist statistics which exploit only the stationary statistics of the observables in the database, HMM also makes use of the temporal pattern of the observables as well. The algorithm also operates in "learning" mode to gradually optimize the HMM. Our technique is designed to operate with or without color data. The version that ingests both panchromatic and color data can accommodate gaps in color photometry data. That attribute is important because while color indices, e.g. Johnson R and B, enhance the quality of the belief (probability) of a hidden state, in real world situations, flux data is collected sporadically in an untasked collect, and color data may be absent. Fluxes are measured with experimental error whose effect on the algorithm will be studied. Photometry data in the AFRL's Geo Color Photometry Catalog (GCPC) and Geo Observations with Latitudinal Diversity Simultaneously (GOLDS) data sets are used to simulate configuration changes and identity cross-tags. The algorithm is tested against simulated sequences of observed magnitudes, mimicking the cadence of untasked ground sensors, configuration changes and cross tags of in-cluster satellites. We would like to show that the on-line algorithm can detect change; sometimes right after the first post-change data point is analyzed. We would like to show the unsupervised "learning" capability that allows the HMM to evolve with time without user's assistance. For example, the users are not required to "label" the true state of the data points.

1. INTRODUCTION

A space surveillance system based on optical sensors often has to deal with the difficulty of identifying satellites when they are closely-spaced as in the geostationary (GEO) orbits. The systems, often relying on automated correlation algorithms, use orbital information derived from metric information to project the positions of the RSOs in the sensor's frame. Using that information, software run at the sensor site associates each detected point source with a catalog identity. However, the identity of the satellites can be cross-tagged because of the uncertainty in the orbital information that may result in misplacing the objects in the sensor's frame. The problem is made more severe by the practice of orbital co-location which is becoming more common in GEO. Co-location is a formation strategy in which two or more satellites share one geostationary longitude range. The International Telecommunications Union (ITU) assigns geostationary orbital longitude slots to operators for the purpose of frequency management. A typical station keeping box is in the order of ~0.1 degrees in longitude and latitude and there are over 20 cluster groupings in GEO. As a result, cross-tags can be introduced by frequent station-keeping, orbital information

2015 AMOSTECH, Sept 14 2015. Public Affairs Release #: 377ABW-2015-0692

uncertainty or the automated processing at the sensor sites. It has been proposed that photometry can help with identifying satellites in those co-location clusters. The idea is to take advantage of the relatively fixed poses of three-axis stabilized geosynchronous satellites and their reproducible light curves, i.e. magnitude versus time. On a typical GEO satellite, the only major appendage that continuously changes orientation consists of the solar panels. They are typically controlled to track the longitude of the sun with a fixed offset angle. The remaining body of the satellite does not move relative to an Earth-fixed frame. As a result of that type of attitude control, the light curve is producible from night to night, at least in a range of epochs for which the solar declination is almost unchanged and as long as the satellite operators do not initiate any configuration changes. Changes are observed but only infrequently. In general, satellites are built differently and as such the light curve of one is different from that of the next. The difference in photometric signatures has been explained in terms of the solar phase angle [Africano, 2005]. Color signatures have been proposed by researchers [Payne, 1996] [Dao, 2008] to distinguish one from another. The implementation of those techniques hasn't been adopted at the operational level for a number of reasons. First and foremost, the optical sensors operated in the space surveillance system are designed to collect metric information. A conversion to robust photometric sensor systems would require a fundamental change in objectives and sometimes infrastructure. A more fundamental issue is the lack of mature automated processing that can ingest photometry data. The difference between expert-based analyses which have been reported and automated processing is substantial. While the SSN can only use a fully automated system to collect, analyze and disseminate data, researchers thus far have only focused on the feasibility of the concepts and not on automation. For example, the research has not addressed the issues of automation and the requirement of an online capability. Reports have been based on study cases with hand-selected data sets. Online processing is the capability of processing sequential data and delivering the assessment with each increment of data. If the objective is to detect changes, the difference between online detection and batch detection (or offline) is that online detection is reckoned with each new datum. Batch techniques, similar to analyses conducted by an expert, are used when one has access to the entire dataset. In an operational SSN, it is not always possible that an analyst has the luxury of time to analyze the entire batch of data and of it is desired to detect the cross-tag as soon as it is made evident by the supporting data. The objective of this study is to show that an algorithm can be used to process the incoming data and generate warning flags of change with quantifiable uncertainty and no latency. Chaudhary proposed a technique based on Bayesian Network to use panchromatic data to detect in near real time the occurrence of cross-tag [Chaudhary, 2014]. This study, also based on a Bayesian network, aims at the development of an algorithm that (a) makes use the concept of differential photometry to alleviate photometry uncertainties, (b) can ingest additional color data to improve detection's accuracy when photometry alone cannot identify the object and (c) learns from data to evolve the probability distributions of the observables. (a) makes the algorithm robust with respect to real life noise such as night to night calibration variability and unaccounted changes in atmospheric extinction (clouds). (b) improves the chance of identifying the object when photometric inform is not discriminating enough. (c) is crucial for optimum automated operation because it lessens the burden of defining a priori information. We rely on proven algorithms to evolve the model parameters of the observables.

2. SIMULATION OF PHOTOMETRY

Photometry data are routinely collected with operational sensors and non-traditional sensors. Color photometry may be collected by the later. AFRL and collaborating organizations have conducted measurements of three-axis-stabilized geostationary satellites in the Geostationary Observations with Latitudinal Diversity Simultaneously (GOLDS) and GEO satellite Color Photometry Catalog (GCPC) efforts. We use the data in these two data sets to construct the signature models and simulate the sequence of photometric signatures of interest. In this study, we focus on the two clusters with high potential of cross-tag : the cluster at 101^{o} W and the AnikF1/AnikF1R cluster at 107.3^{o} W.

The GOLDS campaign was conducted in two phases, both lead by AFRL's Space Vehicles Directorate with the participation of a consortium of organizations [Fulcoly, 2003]. The objective was to investigate the seasonal dependence and latitudinal dependence of the photometry of representative stable geostationary satellites. In

GOLDS II, eight telescopes at five locations across the United States from northern Virginia to Maui (Figure 1) are used.
GCPC and GOLDS data share the same format and collection parameters. When combined, they provided us with a comprehensive catalog of high cadence light curves. The data for the 101 º W and Anik cluster satellites are compiled to form a fidelity data set used to construct the signature models of the mentioned satellites. Because light curves change continuously as a function of day of year, we chose the appropriate range of epochs to ensure that the signature models are valid for a given epoch. We want to simulate the signatures of those satellites for a period of five to ten days from the selected epoch. It is expected that the models stay valid for that period of simulation.
GCPC data is used to simulate the Anik F1 and Anik F1R satellites.

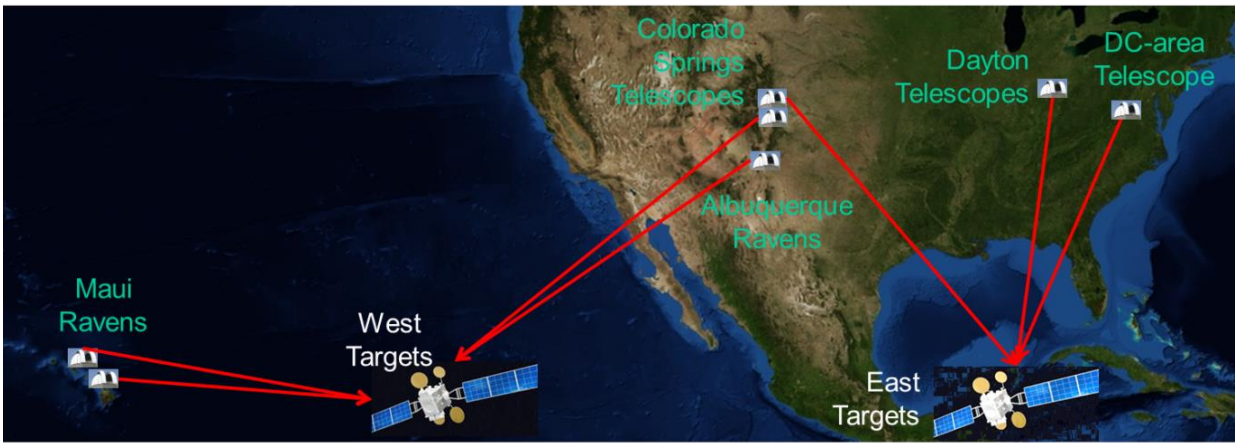

Figure 1. Typical configuration of ground-based sensors participating in the GOLD campaign.

The plots in Figure 2 show the light curves used as models for the satellites in the 101 º W cluster: DTV4s (SSN 26985), DTV8 (SSN 28659), DTV9s (SSN 29494) and SES1 (SSN 36516). The telescopes participating in the GOLDS campaigns operate with the Johnson R and Johnson B filters. These filters are also referred to as the Johnson-Cousins UBVRI system. As mentioned earlier we would like to test a technique developed for automated detection of change using open band photometry and open band with color augmentation. The JR brightness values are used instead of open band brightness when we do not have open band measurements. This substitution is justifiable because the JR band overlaps well with the convolved efficiency curve of the CCD detector and solar spectrum. For color photometry, we use the JB brightness. The choice of JB may not be optimum for differentiating satellites and should be investigated further with respected to on-line automated identification. Previous research by [Payne, 2002] shows that the JB and JR color indices can be used for differentiation when the analysis is conducted by analysts using entire light curves. This type of analysis, referred to in this paper as batch analysis relies on data of moderate to high cadence covering a wide range of solar phase angles. For on-line detection of change, we assume that those same filters can be used but that assumption needs to be validated and it is outside the scope of this study.
The model light curves of Anik F1 (SSN 26624) and Anik F1R (SSN 28868) are shown in Figure 3. These models are based on the average light curves collected on those satellites and contained in the GCPC catalog.

1. HIDDEN MARKOV MODEL

The proposed technique to calculate the probability of change or cross-tag is based on Bayesian network. The objective of the analysis is to estimate the probability that the identity of a given satellite was correctly labeled or correct orbital information was provided for it. To accomplish that objective, we use the technique of Hidden Markov Model (HMM) which is a common tool to model time-series data. A fundamental discussion of the theory is beyond the scope of this paper.

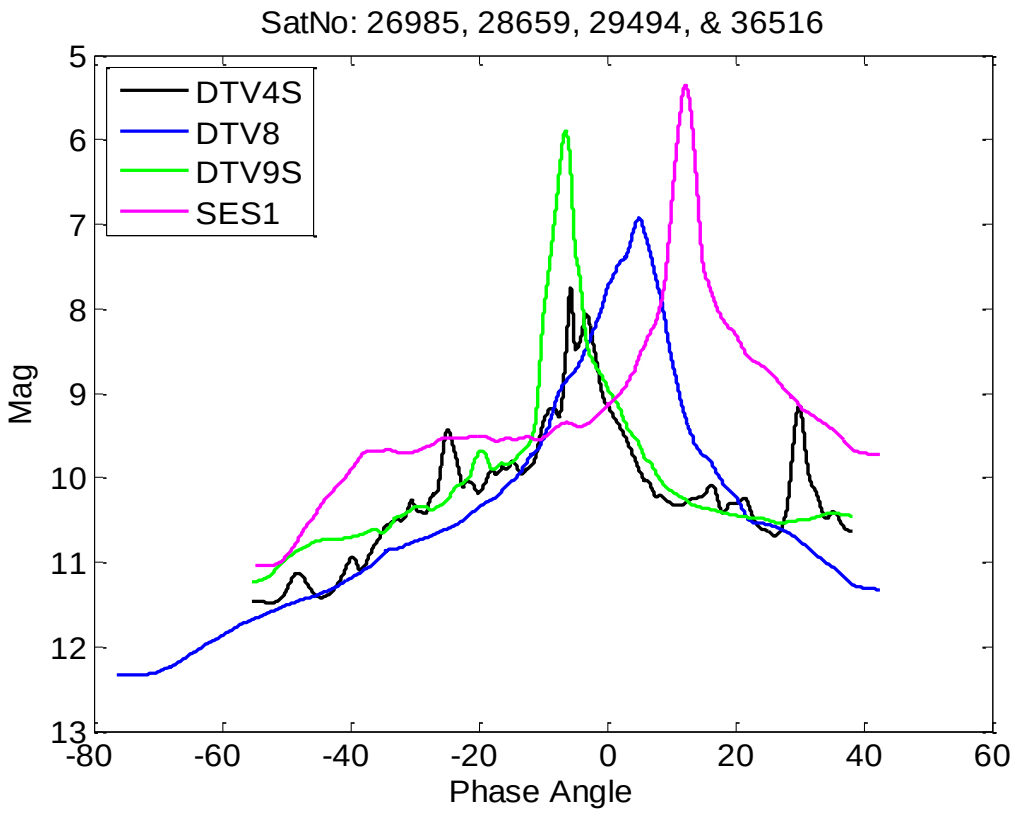

Figure 2. Panchromatic magnitude light curves for the four satellites in the 101 W ^{o} cluster.

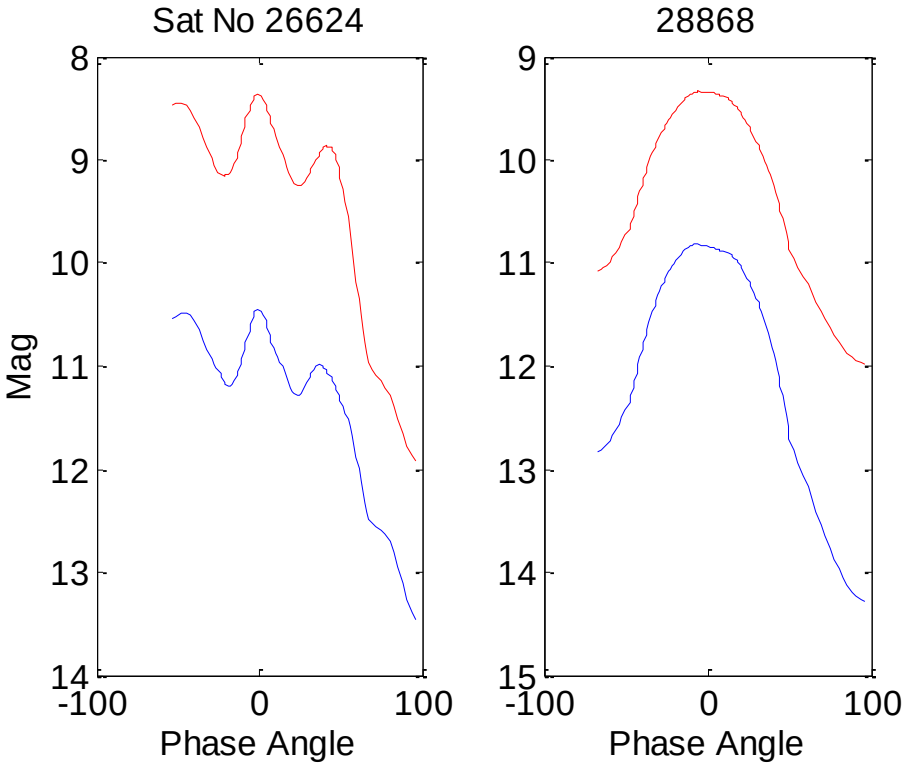

Figure 3. JR and JB magnitudes or light curves for Anik F1 and Anik F1R.

The seminal paper by Rabiner [Rabiner, 1989] provides an excellent introduction. We chose to represent the dynamic HMM as a graphical model of the Bayesian network in Figure 4.

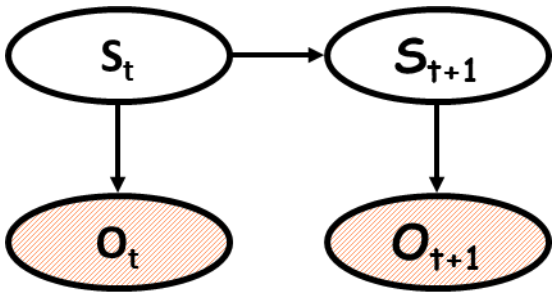

Figure 4. Directed acyclic graph of a dynamic Hidden Markov Model.

Ground-based sensors are used to collect photometric data on three-axis stabilized geostationary satellites. The observations O_t, derived from photometry, are sampled at more or less equally-spaced time intervals. Under those circumstances, time t can be replaced with an integer-value index. Each observation produces one or more observable variables which are derived from photometry and color (if available) data in manners that will be discussed and defined later. The observation at time t was determined by a process whose state S_t is hidden from the analyst. Furthermore, the hidden process is assumed to have the Markov property, meaning the current state S_t depends only on sate S_{t-1} and not on any states before $t-1$. That property allows us to represent the model as shown in Figure 4. The model encapsulates all statistical interdependencies between the variables and fundamentally determines the manner the dHMM calculates. In our analysis, the state S can have two discrete values: 1 if the satellite's label is correct and 2 if the label is incorrect, due to a change. The change could result from a cross-tag between two objects in the same cluster or an intrinsic signature change (e.g., solar panel reorientation). We use the dHMM is to estimate the hidden state based on the sequence of observables.

There are two approaches to statistics: frequentist and Bayesian statistics. We argue that the Bayesian framework is superior to the frequentist's approach in this problem because the technique begins with an initial (prior) knowledge of the dHMM and continuously revises the probability of the hypothesis using evidence contained in the data. In contrast, in the frequentist's view, the model's parameters are fixed and the data set is strictly viewed as a random sample. In the Bayesian's view, the data set is fixed and the parameters are variable. The ability for Bayesian inference to update prior probability and generate a posterior probability (and all estimates derived from it) is an important benefit. Applying the dynamic Hidden Markov Model on time series is straightforward and has been used for speech recognition [Baker, 1975] and many other fields.

In this study, the real-valued observables are modeled as having Gaussian conditional probability distributions (CPD). As shown later, the observables are not strictly Gaussian distributed but this violation of the assumption has not been harmful to the effectiveness of the technique. An HMM is a 5-tuple λ defined as in (2). N is the number of states which are generally hidden from the observers. For example, the true state of the satellite's tag is not known to the observer. It was provided in the orbital element set but from the observer's perspective, that information may be wrong. The observables are defined from measurements in a manner that emphasizes the difference between the different states. As discussed later, the definition of the observables is also tailored for specific identification of the hidden state. In this example, N is 2 for the two states: correct tagging and incorrect tagging (or cross-tag with respect to a given pair of satellites). We can also choose N to be 4 for the following states: 1=correct tagging, 2=cross-tag between 1 and 2, 3=cross-tag between 1 and 3, etc. We found that our technique is more efficient in resolving the cross-tags by calculating the belief ("probability") of cross-tag by inspecting one pair at a time (N=2). For each set of measurements, we would then run the dHMM multiple times to analyze all possible cross-tags.

$$
\begin{aligned}
&\lambda = \langle N, M, \{\pi_i\}, \{a_{ij}\}, \{b_i(k)\}\rangle \\
&N = number\ of\ states\ (hidden) \\
&M = number\ of\ observables \\
&i, j = 1..N \quad k = 1..M \quad y \in \Re \\
&\pi = prior\ probability\ \pi_i = P(q_1 = S_i) \\
&a = state\ transition\ probability\ a_{ij} = P(q_{t+1} = S_j \mid q_t = S_i) \\
&b = observation\ probability\ b_{ik}(y,t) = P(O_{kt} = y \mid q_t = S_i)
\end{aligned}
\tag{1}
$$

The building of the dHHM consists of specifying the vector initial probability of the states π_i, the (*NxN*) matrix of transition probabilities a_{ij} and the *(NxM)* observation probability b_{ik}. The latter, sometimes referred to as output model, is the Gaussian CPD for each value of the hidden state. When an observable is a real-valued variable than can be approximated as a Gaussian distributed, b_{ik} can be defined as the matrices of mean and covariance. Therefore, *b* is the (*NxMx2*) matrix $\{\mu_{ik}, \sigma_{ik}\}$. Table 1 shows all the dHMM parameters initially assumed for the case described in Section 4 for the pair of DTV4s and DTV8 and the same values at the conclusion of the analysis at data point #100. Note at each time step, the Expectation Maximization algorithm is applied to iteratively find the maximum likelihood or maximum a posteriori (MAP) estimates of the parameters the probabilistic model λ. At each step, EM will update the model. The parameters learned from the data at the end of the analysis is shown in the table as learned parameters [Dempster, 1977]. Because the parameters evolve with further ingestion of data, the importance of the initial estimates gradually diminishes and eventually λ is dominated by data. In this study, that transition generally occurs at time step #10 approximately. The discussions on how to estimate the initial parameters will be given in Section 4.

Table 1. Probabilistic model parameters

	Initial transition probability			Initial mean		Initial sigma					
	S=1	S=2		S=1	S=2	S=1			S=2		
						Obs 1	Obs 2	Obs 3	Obs 1	Obs 2	Obs 3
S=1	0.950	0.050	Obs 1	0.000	-0.290	0.070	0.000	0.000	1.905	0.000	0.000
S=2	0.050	0.950	Obs 2	0.000	-0.145	0.000	0.070	0.000	0.000	0.953	0.000
			Obs 3	0.000	-0.145	0.000	0.000	0.070	0.000	0.000	0.953
	Learned transition probability			Learned mean (t=100)		Learned sigma (t=100)					
S=1	0.900	0 .100	Obs 1	0.005	-0.515	0.023	0.006	0.006	4.571	2.273	2.289
S=2	0.143	0.856	Obs 2	0.016	-0.257	0.006	0.017	0.004	2.273	1.147	1.143
			Obs 3	0.012	-0.272	0.006	0.004	0.016	2.289	1.143	1.163

A Hidden Markov Model (HMM) is a probabilistic function of a Markov property. The term "hidden" indicates that the system is a doubly stochastic process where the state $q_1^t = \{q_1, \cdots\cdots, q_t\}$ of the Markov chain is not directly observed, but it is implicitly defined by a sequence $o_1^t = \{o_1, \cdots\cdots, o_t\}$ of observables that do not necessarily have the Markov property. Given the state q_t, the distribution of o_t is independent of other variables,

$$
P(o_t \mid q_1^t, o_1^{t-1}) = P(o_t \mid q_t) \tag{2}
$$

Furthermore, o_t cannot affect q_t given the past.

$$P\left(q_{t+1}\middle|q_1^t, o_1^t\right) = P\left(q_{t+1}\middle|q_t\right) \qquad (3)$$

One of the important tasks is to find the probability of a sequence of observations. The probability of the observed sequence, written as $P\left(y_1^T\right)$ for all T steps, can be calculated by finding the joint probability of the observation sequence and the state sequence $P\left(y_1^T, q_1^T\right)$ using conditional probabilities and the chain rule.

$$\begin{aligned} P\left(o_1^T, q_1^T\right) &= P\left(o_T, q_T\middle|o_1^{T-1}, q_1^{T-1}\right) P\left(o_1^{T-1}, q_1^{T-1}\right) \\ &= P\left(o_T\middle|q_T, o_1^{T-1}, q_1^{T-1}\right) P\left(q_T\middle|o_1^{T-1}, q_1^{T-1}\right) P\left(o_1^{T-1}, q_1^{T-1}\right) \\ &= P\left(o_T\middle|q_T\right) P\left(q_T\middle|q_{T-1}\right) P\left(o_1^{T-1}, q_1^{T-1}\right) \\ &= P(q_1)\prod_{t=2}^{T} P\left(q_t\middle|q_{t-1}\right)\prod_{t=1}^{T} P\left(o_t\middle|q_t\right) \end{aligned} \qquad (4)$$

where

$P\left(q_1\right)$ is the initial state probability distribution of *q* at time *t*

$P\left(q_t\middle|q_{t-1}\right)$ is the probability of *q* at time *t* given *q* at time *t+1*

$P\left(o_t\middle|q_t\right)$ is the emission or observation probability

We can get the desired probability by marginalizing (summing) over random variables

$$q_{1..T} : P(o_1^T) = \sum_{q_{1..T}} P\left(o_1^T, q_1^T\right) \qquad (5)$$

The direct approach of using (4) is computationally difficult since it has an exponential order of complexity, $(2T-1)N^T$. For an HMM with two hidden states and 100 time steps, the simplest case in this study, the number of calculations required to calculate the probability of an observed sequence is 2.5×10^{32}. Instead, we can calculate the joint probability using an alternative method called the forward-backward algorithm [Rabiner, 1989]. This multi-pass algorithm reduces the complexity of the computation. We are also interested in finding the most likely sequence of states q_1^T corresponding to a given sequence of observables o_1^T. The state posterior probability $P\left(q_t\middle|o_1^T\right)$ is the probability of being in a certain state at time *t*, given the observation sequence. It can be expressed using the variables that we defined in the forward-backward calculations.

The probability $P\left(q_t\middle|o_1^T\right)$ is the product of forward-backward variables and normalized by the joint distribution of the observation sequences. The following equation is used to express it.

$$P\left(q_t\middle|o_1^T\right) = \frac{P\left(q_t, o_1^T\right)}{P\left(o_1^T\right)} = \frac{P\left(o_1^t\middle|q_t\right)P\left(q_t\right)P\left(o_{t+1}^T\middle|q_t\right)}{P\left(o_1^T\right)} = \frac{P\left(o_1^t\middle|q_t\right)P\left(o_{t+1}^T,\middle|q_t\right)}{P\left(o_1^T\right)} \qquad (6)$$

Since $P\left(q_t\middle|o_1^T\right)$ is normalized by the joint distribution of the observation sequences, i.e. $\sum P\left(q_t\middle|o_1^T\right)=1$. The most likely state can be estimated by maximizing $P\left(q_t\middle|o_1^T\right)$ for a given q_t. The probability of a given state is called belief as in the literature of Bayesian Network. A belief close to 1 indicates a strong belief that the state is correct. To improve the accuracy of the HMM, we also learn from data to improve the parameters, however, the discussion of reevaluating the parameters is outside the scope of this paper. The reader can refer to this excellent reference article [Bengio, 1999].

Detection of cross-tags is typically performed using orbital metric information. The feasibility of photometric cross-tag detection by expert-based analyses has been proposed by [Payne, 2002]. In [Chaudhary, 2013] an HMM technique based on a single observable has been proposed to detect a cross-tag between two objects. This study explores for the first time the use of multiple observables because o_1^T can be a sequence of vectors, observables based on color photometry and observables based on differential magnitudes. The color augmentation improves the

effectiveness of the HMM whenever color photometry is available. A comparison between Bayesian belief and truth data will show the improvement. The last improvement is the use of differential magnitude to improve the robustness of the dHMM with respect to the contamination of real life noise such as the effects of aerosols and thin clouds.

2. Panchromatic dHMM technique and results

All optical sensors, operated with CCD array, can provide satellite photometry by integrating the signal in the pixels associated with it. Since the objective of this study is to investigate the detection of cross-tags, we only consider the case when all the co-located satellites in the cluster are measured in the same field of view. It is reasonably assumed that their photometric signals can be collected simultaneously. In this case, unless atmospheric extinction can vary at a scale less than the angular separation of the objects, typically tenths of a degree, it's reasonable to assume that the extinction is the same for all objects. This property of a common atmospheric extinction can be exploited to mitigate the uncertainty in measured magnitudes.

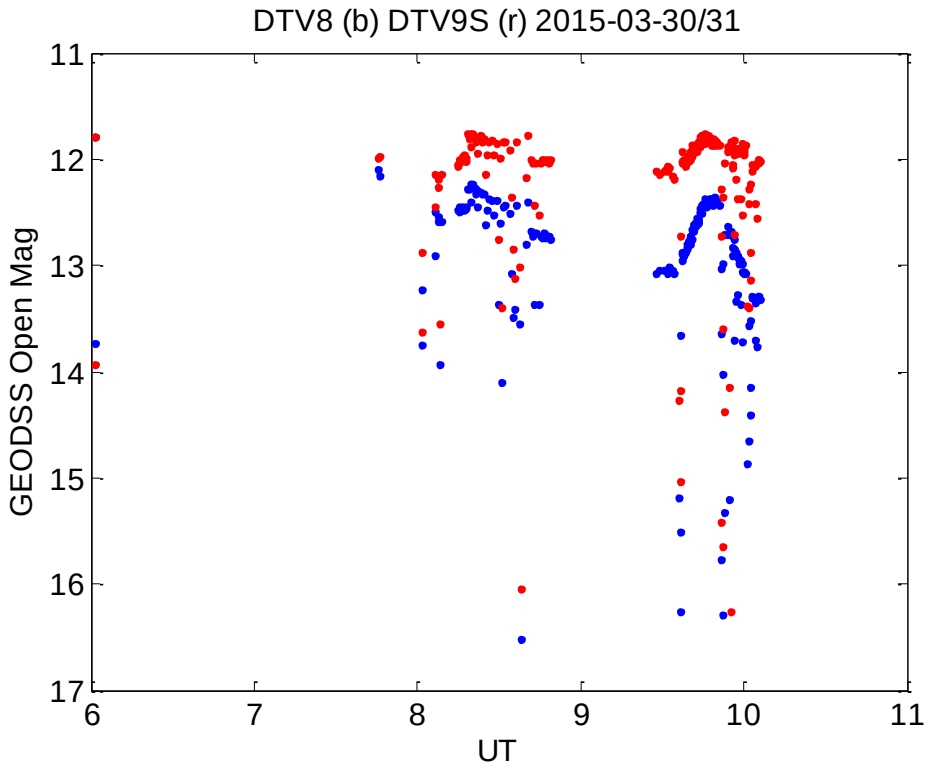

Figure 5. Magnitudes of DTV8 and DTV9S. Both satellites are in the 101 W cluster.

In Figure 5, the magnitudes of Direct TV8 (DTV8) and Direct TV9s (DTV9s), collected on 03-31-2015, between 6:00 and 10:00 UT, are shown as a function of time (UT). The night of 3-30 and morning of 3-31, there were scattered clouds in the area of Colorado Springs where the Yoder test site's telescope is located. The expected light curve is a modulating curve that peaks at 9:50 and varying between 12 and 13.4 in magnitude. The passage of clouds and increase in atmospheric extinction is marked by data gaps around 6:00-8:00 and 8:45-9:30 UT. In these gaps, the extinction is so high and the objects so dim that the signatures could not be recorded. At other times, the magnitudes were recorded albeit with extinction, corresponding to increases of magnitude of up to 3 (dimming). The affected data points are recognized in Figure 5 as those points that deviate from the expected light curve by as much as 3 magnitudes -downward in the plot. Of course, one cannot predict which points are affected by cloud extinction and therefore errors as large as 3 magnitudes are present in this collect. In contrast, careful photometric calibration

in a cloudless night is claimed to produce magnitudes with standard error of 0.1 or better. However, in less ideal conditions, the error is dominated by actual atmospheric extinction effects. As noted earlier, while the object's magnitude is affected by clouds, the differential magnitude, defined as the difference between objects' magnitudes in the same field of view is not directly affected by atmospheric extinction. Of course, the extinction will reduce the SNR of each measurement of magnitude, reduce the differential magnitude's SNR and increase the signal-limited contribution to magnitude noise.

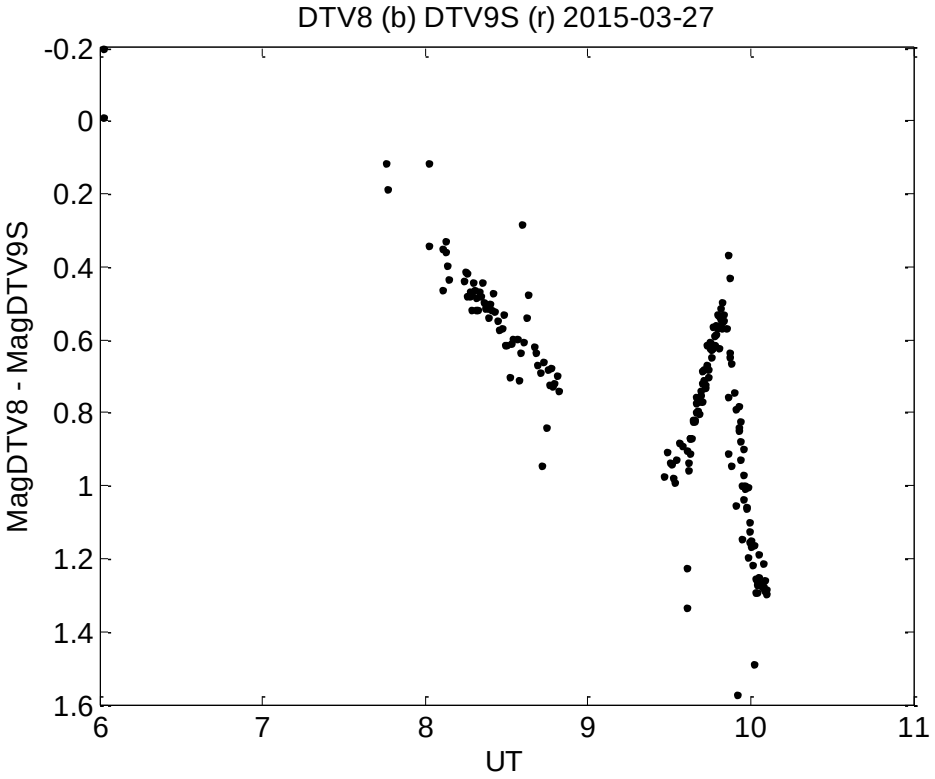

Figure 6. Differential magnitude of DTV8 (relative to DTV9S). Both satellites are in the 101^{o} W cluster.

Figure 6 shows the differential magnitude of DTV8 (relative to DTV9s). The data points follow a noticeable downward trend from 7:40 to 8:40 and a peak at 9:50. The peak in differential magnitude is due the peak in the DTV8 light curve. The average deviation of the data points from the observed trend is about 0.05 magnitudes though there are a few data points as much as +/-0.3 mag away from the trend. Those outliers could be due to the non-uniform distribution of cloud attenuators within the field of view. The 0.05 mag standard deviation is approximately 1.4 times the standard deviation of the magnitudes seen in Figure 5 when we consider only portions of the light curve not affected by clouds. The standard deviation of ~0.05 is therefore identified as the noise of the differential magnitude. We concluded that the standard deviation of the differential magnitudes is ~1.4 times that of the cloudless magnitudes and much smaller than noise due to clouds. The question that remains to be answered is how can we use the differential magnitude for cross-tag detection.

Without loss of generality, we use the specific case of the 101^{o} W cluster. Referring to the magnitudes of co-located satellites as m_{i}, with $i=1..4$, the observables as o_j, $j=1..3$, the definitions are as followed.

$$
\begin{aligned}
o_1 &\equiv m_1 - m_2 - \hat{m}_1 + \hat{m}_2 = \begin{cases} \varepsilon_1 - \varepsilon_2 \quad (No\ crosstag) \\ m_2 - m_1 - \hat{m}_1 + \hat{m}_2 (1 \leftrightarrow 2\ crosstag) \end{cases} \rightarrow \begin{cases} \mu_{11} \approx 0 \quad \sigma_{11} \approx \sqrt{2}\varepsilon \\ \mu_{12} \approx 2 \cdot mean(m_2 - m_1) \end{cases} \\
o_2 &\equiv m_1 - m_3 - \hat{m}_1 + \hat{m}_3 = \begin{cases} \varepsilon_1 - \varepsilon_3 \quad (No\ crosstag) \\ m_2 - m_3 - \hat{m}_1 + \hat{m}_3 (1 \leftrightarrow 2\ crosstag) \end{cases} \rightarrow \begin{cases} \mu_{21} \approx 0 \quad \sigma_{21} \approx \sqrt{2}\varepsilon \\ \mu_{22} \approx mean(m_2 - m_1) \end{cases} \\
o_3 &\equiv m_1 - m_4 - \hat{m}_1 + \hat{m}_4 = \begin{cases} \varepsilon_1 - \varepsilon_3 \quad (No\ crosstag) \\ m_2 - m_4 - \hat{m}_1 + \hat{m}_4 (1 \leftrightarrow 2\ crosstag) \end{cases} \rightarrow \begin{cases} \mu_{31} \approx 0 \quad \sigma_{31} \approx \sqrt{2}\varepsilon \\ \mu_{32} \approx mean(m_2 - m_1) \end{cases}
\end{aligned}
\tag{7}
$$

$\hat{m} = \exp ected\ value\ of\ magnitude\ m$

$\varepsilon = std\ deviation\ of\ zero\ meaned\ noise$

$\mu = mean\ of\ observable$

$\sigma = \mathrm{cov}\ matrix\ of\ observables$

The definition of the observables and estimates of their means and covariances are provided in Equation 7. Note that the HMM observables, defined from measured quantities, may not be direct measurements but quantities derived from measurement. The values of the observables are shown for the case S=1 (correct tag) and S=2 (satellite 1 is cross-tagged with 2) in the middle bracket. In the rightmost brackets, the expected mean and covariance of the observables are estimated. The expected value of the mean of the differential magnitude m_2-m_1, are estimated from the empirical light curves. These means and covariances are used as the initial prior CPDs for the corresponding values of the hidden state. For brevity, the expressions of the covariance for S=2 are left out of the equation. It can also be calculated using the empirical light curves. While the initial CPDs are required to start the dynamic HMM, new data will gradually overcome a priori information. Most conventional data fusion algorithms have probabilistic models as a key component. The use of all three observables to infer the Bayesian belief (equivalent to probability) of each the two hidden states is also known as Bayesian data fusion. By including all relevant observables, we unify the statistical analyses of the observables. The relation between the hidden state and the observables is automatically considered. The particular choices of observables are crucial to the effectiveness of the dHMM in calculating cross-tag belief. The expression of the observables, as shown in Equation 7, warrants that all three observables will have a zero mean for S=1 and finite mean for S=2. The choice results in a strong distinction between a correct tag and an incorrect tag. With this mode of operation, the cross-tag is only considered between satellite 1 and 2. To estimate the belief of all cross-tags, the dHMM is run multiples times to cover all permutations of satellite 1 and 2. Satellite 1 can be any of the 4 possible satellites. Satellite 2 can be any of the three remaining satellites. Other modes of operation require the number of hidden states to be larger than two so one can infer the identity of the cross-tag partner without running the algorithms multiple times. A comparison of the many approaches will not be discussed.

In this test, the sensors provide panchromatic or broadband magnitudes. It is assumed that each time step, all four magnitudes are collected and analyzed instantaneously. For each satellite, the panchromatic dHMM is used to estimate the belief of correct tagging and cross-tagging with each of the other satellites. As mentioned, the dHMM we described has two hidden discrete states and three continuous-valued observables. It can be run in multiplex to provide the belief of crosstag with each of the three other satellites. The test consists of running the dHHM in two modes: inference and learning. The algorithms used in this study are derived from the Hidden Markov Model Toolbox made available by [Murphy].

The test data set is simulated using the empirical signature models described in Section 2 and shown in Figure 2 and 3. The cadence of the simulated data collection assumes 20 photometric measurements per night, and a total of five nights. The exact times of each measurement are dithered to simulate the fact that operational sensors have to negotiate tasking conflicts and cannot honor the observation requests at exact times. The effect of this randomness results in a distribution of longitudinal phase angles as shown in Figure 7. The tests were also conducted with

cadence varying from 5 measurements per night to 100 measurements per night. While those results will not be reported, we did not see any systematic trends in the performance of the dHMM.

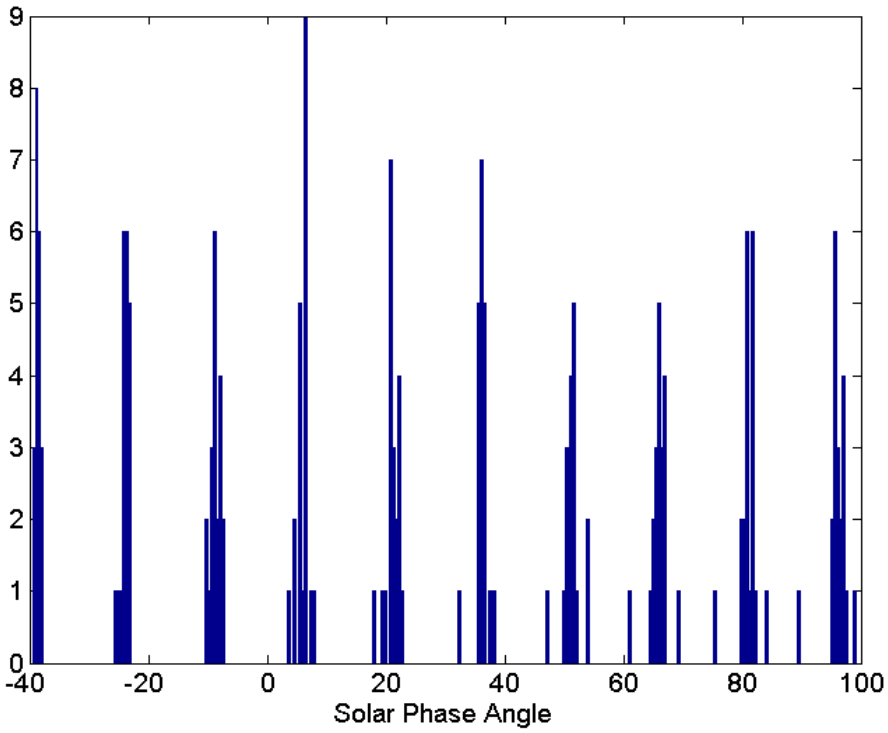

Figure 7. Histogram of solar phase angles of the satellite during the simulated data campaign.

The apparent visual magnitude m_{app} of a satellite is calculated as follows.

$$m_{app}(v) = M_{sun}(v) - 2.5 \log\left(\frac{F_{app}(v)}{F_{sun}(v)}\right) \tag{8}$$

The variable *v* is the band of the sensor. M_{sun} is the Sun's magnitude. F_{app} is the flux of the space object and F_{sun} is the solar flux. The expression of the normalized magnitude M_{abs} is given by the following expression.

$$M_{abs}(v) = m_{app}(v) - 5.0 \log\left(\frac{R}{R_0}\right) - 5.0 \log\left(\frac{R_{sun}}{R_{sun}(1AU)}\right) \tag{9}$$

R_{sun} is the distance to the Sun, R the distance to the GEO object, and R_0 a standard distance for the GEO belt. The last term on the right hand side can be neglected.

When clouds and aerosols are present, the extinction in the object's line of sight may be different from that of the calibration stars. Typically, the stars are measured at a time when the atmosphere is clear and the space objects may be observed with thin clouds in the line of sight. In this scenario, the apparent magnitude is dimmer than the true value. However, if all the co-located objects in the cluster are obscured by the same layer of cloud, the magnitude of each object is increased by the same amount. As a result, the measured differential magnitude is much less affected by cloud's obscuration. In the test data, the atmosphere contains clouds in 20% of the observation time. The

attenuation of the clouds is selected randomly. Using those conditions, the sim-measured magnitudes of DTV4s (satno. 26985) and DTV8 (satno. 28659) are as shown in Fig. 8.

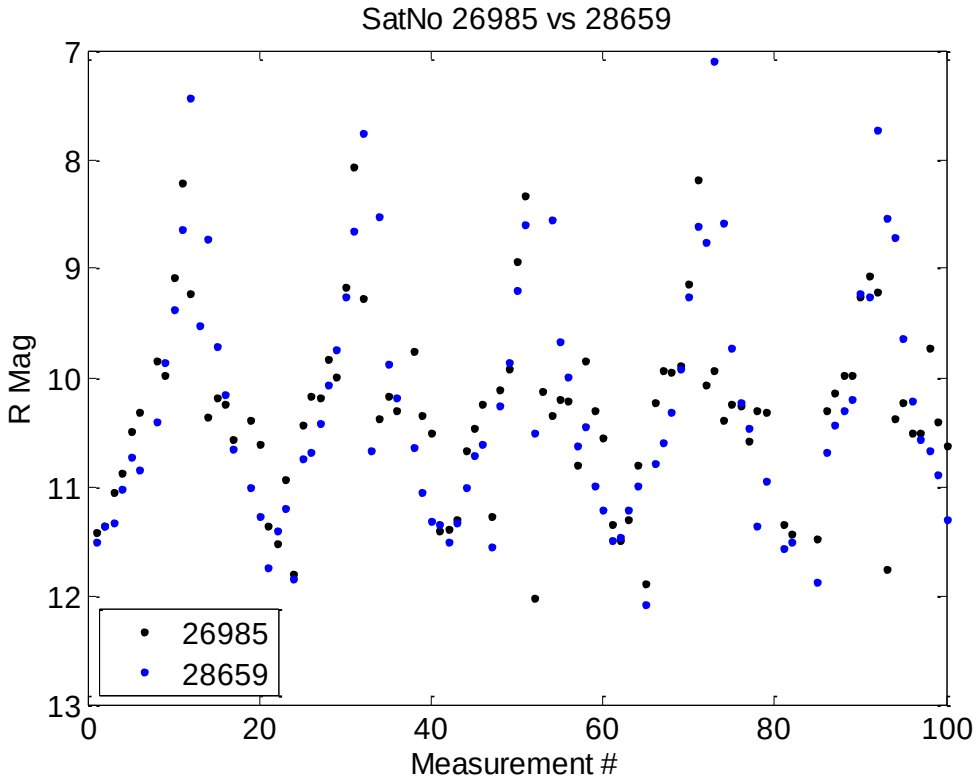

Figure 8. Simulated magnitudes for DTV4S (Satno. 26985) and DTV8 (Satno. 28659). Because of random noise introduced to mimic the effects of sensor and atmospheric extinction noise, it is difficult to distinguish the sequences.

Notice the effect of the intrinsic 0.1 standard deviation due to measurement noise and the presence of many data points that are much dimmer than the empirical light curve. For those points, the deviations can be as much as 3 magnitudes dimmer. The plot in Figure 8 shows magnitude as a function of the observation time index (not time) so it appears as if data is collected continuously. In reality, the groups of measurements (20) are separated by gaps of approximately 12 hours, when observation is interrupted because of the daytime solar background.
Figure 9 (upper panel) shows the sequence of measured magnitudes associated with satno. 26985. A cross tag with satno. 28659 was introduced in the second night of the simulation window, or data point #32. The cross tag was removed later and the magnitude of the correctly tagged magnitude is shown at data point #78. The Expectation-Maximization algorithm [Dempster, 1977] was used to estimate of the parameters of the statistical models, as defined in Equation (1). The belief of correct tagging is calculated after the EM step. The green points represent the Bayesian belief that the hidden state is 1 or the tag is correct. Setting a threshold at 50%, meaning a belief less than 0.5 indicates a cross-tag between the two satellites, results in an on-line prediction which is 97% accurate for this particular sequence of measurements and cross-tag scenario. We proceed to repeat the run by assigning each satellite of the cluster to the place of satellite 1 and each of the remaining three to the place of satellite 2. This technique of running multiple pairs of satellites is used and reported in this paper but there are other configurations are also applicable. For example, the dHMM can be set up to detect the identities of the cross tag partners in a single iteration by increasing the number of hidden states.

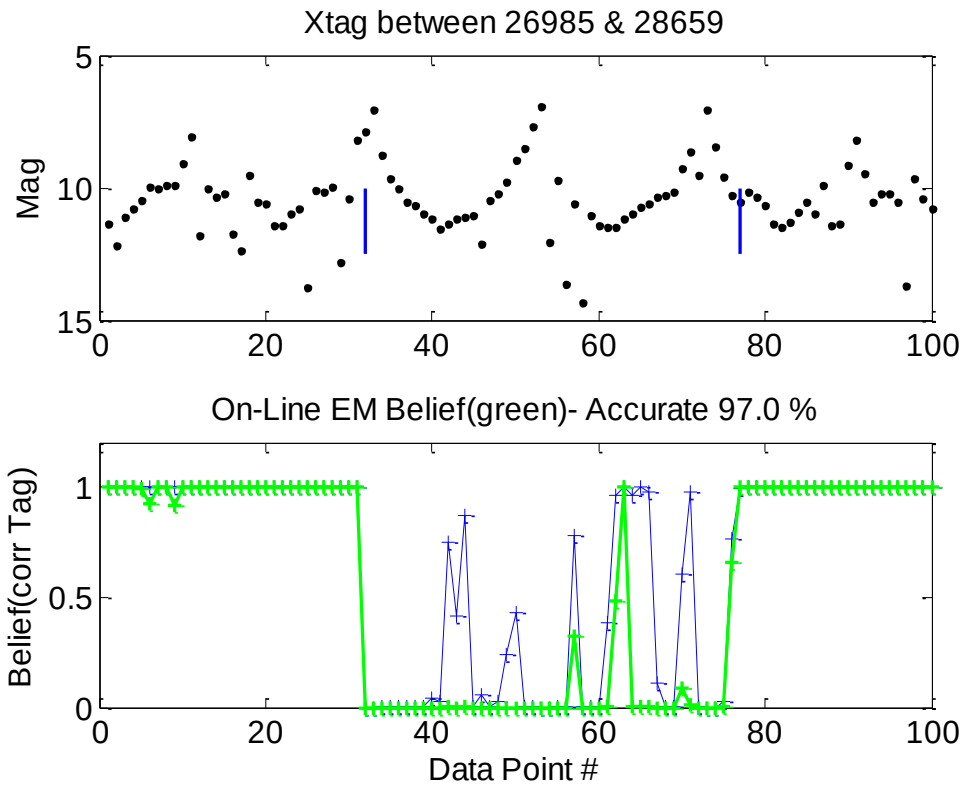

Figure 9. On-line belief of the correct-tag states for the entire simulated window, with respect to cross-tagging between DTV4S (Satno. 26985) and DTV8 (Satno. 28659). The cross-tag was introduced at the time step marked by the left vertical line in the upper panel. The cross-tag was removed at the step marked by the second vertical line. The accuracy of the belief is specific for this run and have a different in the next run because noise is introduced stochastically.

We also found that using the two-state hidden node is most effective in detecting the correct tag state. The results of such a run are outside the scope of this paper. Figure 10 shows the accuracies of cross-tag detection for all possible combinations of cross-tag partners. The dHMM reveals the true state of the tag through the value of the belief of correct tage. As the equivalent of probability, a belief of 1 indicates that the tag is very likely to be correct (no cross-tag). A belief of 0 means that it very likely that object 1 and 2 are cross-tagged. By using an arbitrary threshold (e.g., 0.5), one can assign a value to the hidden state. When the belief is neither near 0 or 1, the assignment does not have high confidence. Since we know the true state of the node at time step, a comparison of the inferred state with the truth can be used to calculate the success or accuracy of dHMM during the entire window of simulation. Note that using a single threshold of 0.5 forces the dHMM to provide an answer at each step. One can choose two distinct thresholds to improve the confidence of the assignment. However, in doing so, the dHMM may not be able to assign a state at each step. This strategy may turn out to be most useful because the dHMM may not be required to provide an assignment unless it has a reliable answer. That trade-off is not considered in this study. Using the single threshold assignment strategy, we can estimate the accuracies of all assignments as in Fig. 10. It's worth noticing that the accuracy is lowest for the pair of DTV4S (26985) and DTV9S (29494). The low accuracy can be explained by the light curves shown in Figure 2. Of the four satellites, DTV4S and DTV9S' light curves are closest in magnitude. At many times or phase angles, their light curves are indistinguishable especially if one has to consider the measurement noise. Including all combinations of crosstags, the average accuracy is 92.6%. The caveat is the simulation is performed for a particular scenario of cross-tag. We did not simulate different scenarios of cross-tags by varying the times when the satellites become cross-tagged. It was mentioned that the most optimum mode of operation is to hold off the tag assignment until the belief is very close to 1 or 0 so we don't have to assign when the indicator is not clear cut. Another mode of operation which is also relevant: running the dHMM in batch mode and providing tag assignments at the end of the night collect. Any delayed reckoning of the tags would result in more accurate assignment.

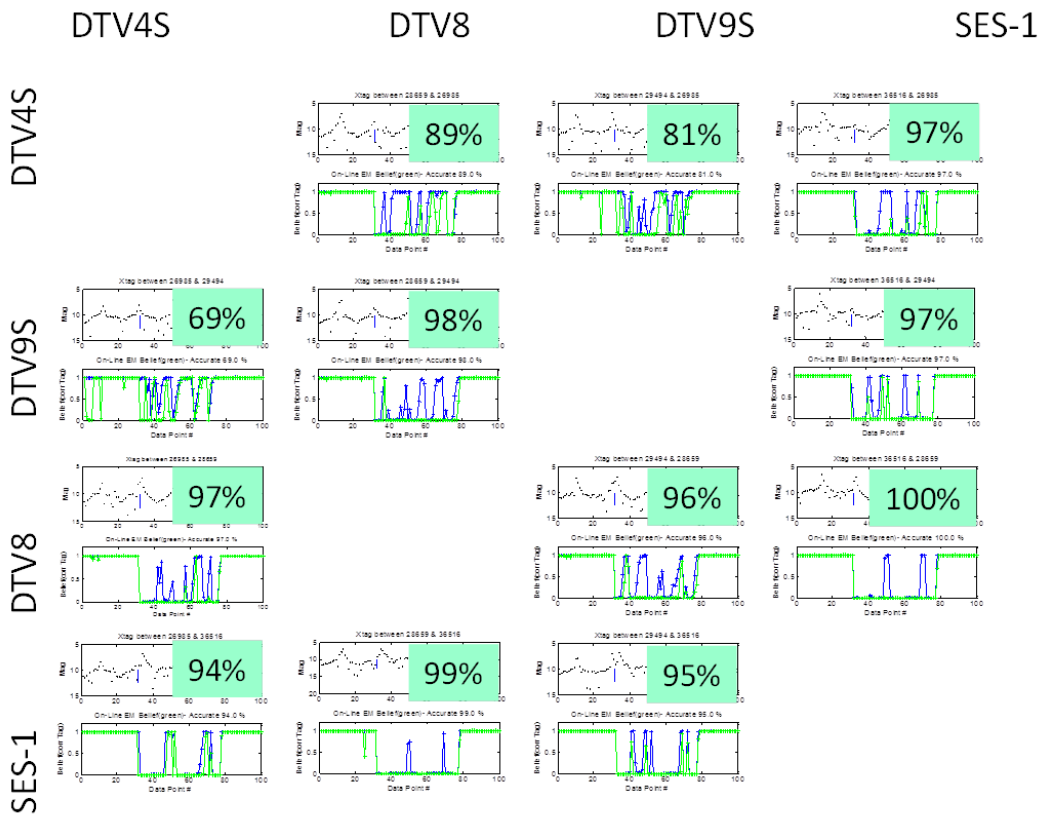

Figure 10. Summary of accuracy of the on-line of cross-tag detection with respect to all the possible pairs of satellites in the cluster.

3. Color dHMM technique: Cross-tag and Solar Panel's Reorientation

With available color photometry, the dHMM can be restructured to accommodate the additional observables. The empirical light curves as shown in Figure 3 are used to simulated 20 nights of measurements. Five magnitudes are acquired each night in the open band and five in the Johnson Blue band. We use the Johnson Red magnitude in the database in lieu of the open band when the later is not available. The magnitudes in those two bands track each other well based on our experience. Additional information always improves the accuracy of the tag assignment by making the belief closer to 1 (or 0). The results of running the dHMM on Anik F1 and Anik F1R satellites are shown in Fig. 11 and 12.

Anik F1 and Anik F1R are co-located in the 107°W cluster and often cross-tagged. The conducted test investigates the benefit of having color photometry. The accuracies of the tag assignment are perfect (100%) with the belief being exactly 1 or 0 when the analysis is done in batch mode. In on-line mode, the belief in the window where cross-tag occurs and the belief should be zero is non-zero at three different time steps. The non-zero values of belief are however quite small and the tag could be correctly assigned. The non-zero value of the belief indicates a lesser level of confidence in the negative state.

To test the ability to detect configuration change, we use the scenario of DTV9S reorienting its solar panel. The GCPC database recorded the light curve before and after such a change, on day 27 and day 30, 2011. The two light curves, shown in Figure 13, are only different in the range of phase angles from -27 to -12 deg. The signature change in that range can be attributed to a reorientation of the solar panel.

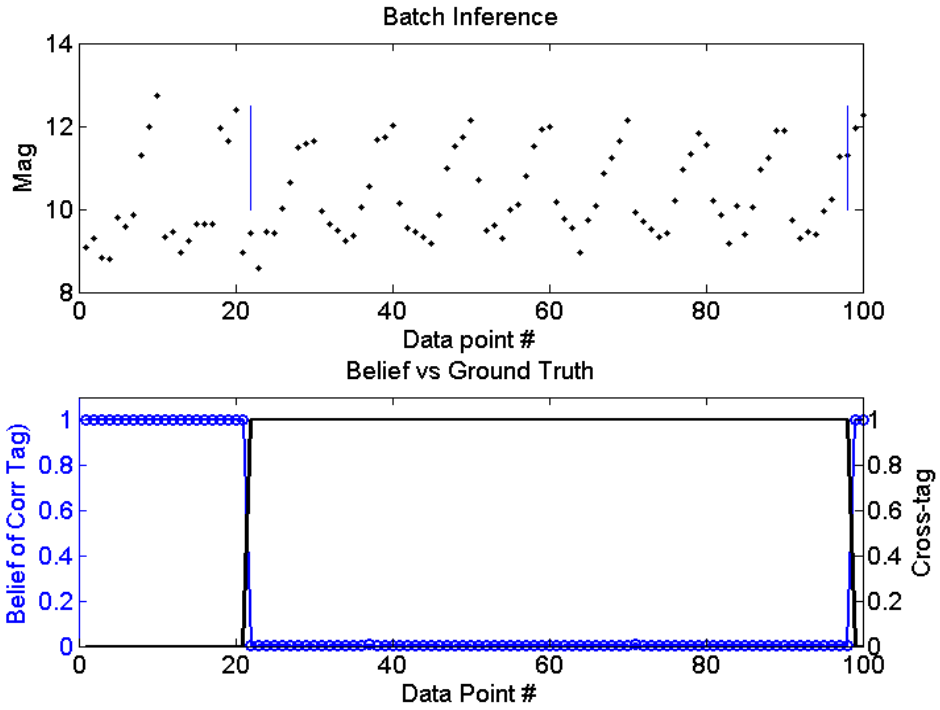

Figure 11. Batch belief of the correct-tag states for the entire simulated window for Anik F1 and Anik F1R . The cross-tag was introduced at the time step marked by the left vertical line in the upper panel. The cross-tag was removed at the step marked by the second vertical line. Batch estimates are perfectly accurate with high confidence levels as shown by the values pinned at 0 and 1.

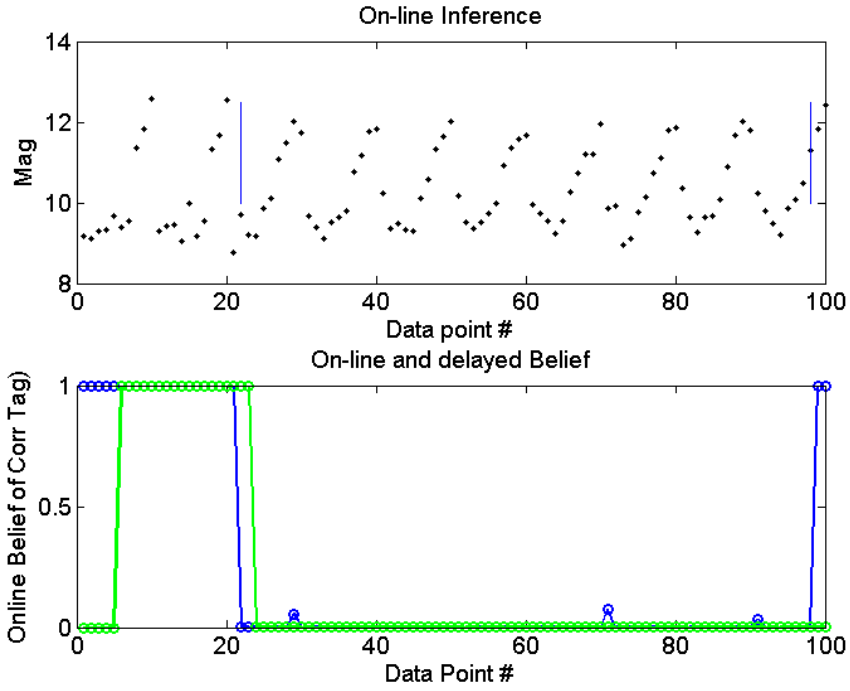

Figure 12. On-line belief of the correct-tag states for the entire simulated window for Anik F1 and Anik F1R . The cross-tag was introduced at the time step marked by the left vertical line in the upper panel. The cross-tag was removed at the step marked by the second vertical line.

Changes such as the one observed with DTV9S, day 27 to day 30, are often observed and on occasions the explanation of solar panel reorientation has been validated by the satellite's operator. For a solar panel that pivots about a North-South axis, the longitude of its normal vector can be aligned with the direction of the Sun for maximum incident solar power. The satellite's operator has the option of steering the panel's normal away from the solar longitude. The amount of steering is called the offset angle. It is customary to have a constant offset angle for a long period. That is the reason for the light curve to be stationary from night to night. The observed light curves are therefore used to simulate a change in solar panel's offset angle. There are 100 sets of photometric data taken over the course of 20 nights. Figure 14 shows the belief of normal behavior or no change. A belief's value near unity indicates high confidence in a normal behavior. Normal behavior means there has been no change. The belief can also indicate an anomalous behavior when its value deviates from unity and approaches zero. It is interesting to note that as soon the solar panel is reoriented, the belief drops to a low value, as expected for a successful and responsive detection. However, the belief does not stay near zero after the initial detection even though the solar panel has been permanently reoriented. It is however explained by the fact that the two light curves are similar outside of the -27 to -12 deg phase angle range where it is difficult for the dHMM to tell the difference. It should be noted the signature model is not allowed to evolve with time in this study. If the solar panel is permanently changed then it makes sense to redefine the normal behavior of the light curve. We did not allow that to happen in this test.

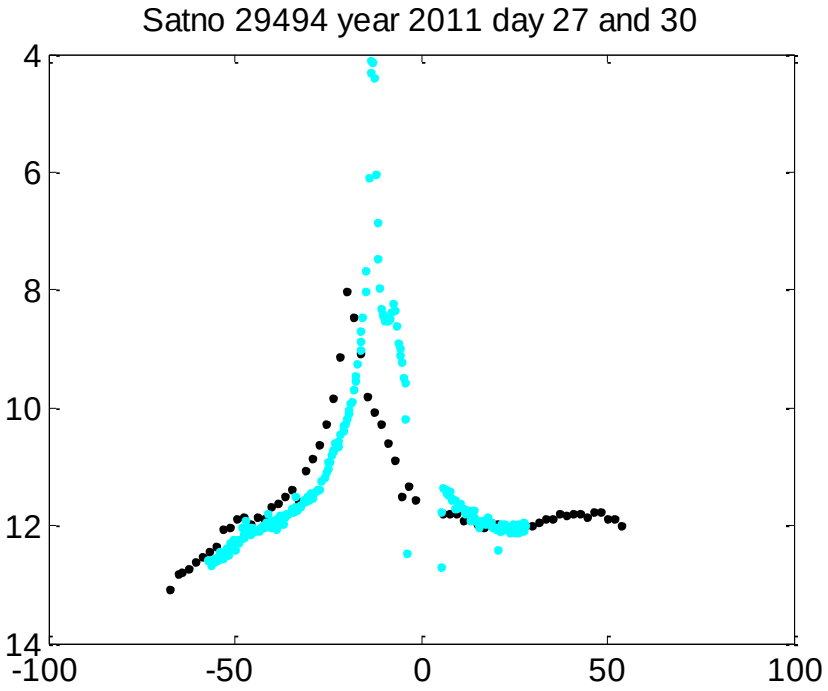

Figure 13. DTV9S light curves before and after solar panel configuration change.

Fig. 14 shows the different light curves collected on DTV9S on day 27 and 30 of 2011. Fig. 14 shows the belief calculated for the simulated change of solar panel offset angle.

4. DISCUSSION AND CONCLUSION

In summary, the investigation of a dHMM-based detection algorithm resulted in encouraging results. The panchromatic dHMM algorithm successfully detected cross-tags in simulated data. The test case of the four satellites in the 101W cluster has confirmed that detection is made with virtually no latency. The algorithm was used in an on-

line cadence, meaning detection is possible with each new photometry datum. The effects of sensor and environmental noise, including that of undetected thin clouds, did not substantially impact the detection algorithm. The accuracy of the on-line detection has been satisfactory (85%) at each time step for the scenario of cross-tag and the conditions described earlier. Batch mode detection is typically more accurate at the expense of latency.
The dHMM that includes additional observables for the color information was tested against the two satellites in the Anik cluster. The color dHMM was shown to detect perfectly cross-tags of Anik F1 and Anik F1R. This capability would be useful if the sensors can provide color filter photometry in the Johnson R and Johnson B, or equivalent bands. The test includes all noise artifacts as described earlier.
The color dHMM was also tested against a simulated reorientation of the solar panel of DTV9S in the 101W cluster. The algorithm was successful in detecting the onset of the reorientation. The differences in light curves between the "before" and "after" satellites occur at a certain range of solar phase angles. This attribute induces a repeating indicators of change every time new data is collected in that range of phase angles. The algorithm is not "aware" it has already detected the change the night before. This mode of detection may not be ideal for end users so we will work on modifying the dHMM to produce a more straightforward indicator of change. Finally, EM learning of the observable probability distribution parameters has been successful in improving the accuracy of the beliefs at a minimum cost in computing time.
In future works, we will use test data collected for test purposes and will have to rely less on data simulated from our historical databases.

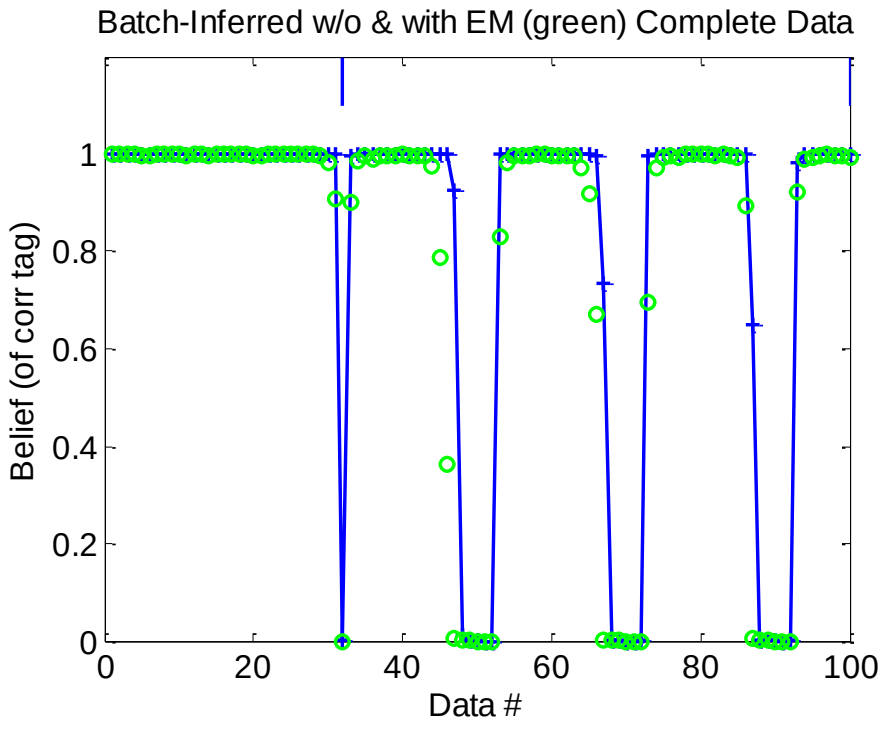

Figure 14. Belief of normal behavior. The blue vertical line indicates the time the light curve changed because of a solar panel reorientation.

ACKNOWLEDGMENT

We acknowledged Mr. Dan Fulcoly, Dr. Jeremy Murray-Krezan, Dr. Steve Gregory, Dr. Tamara Payne, and Dr. Philip Castro for the use of the GOLDS, GCPC and GEODSS data. The motivation and support of Ms. Amber Anderson, the DTIC and DSS teams are indispensable to this effort.

REFERENCES

Africano, J., et al., *Understanding Photometric Phase Angle Corrections*, Proc. of the Fourth European Conference on Space Debris, 2005.

Payne, T. E., et al., *Modeling of Spectral Signatures from GEO Satellites (U),* Presented at the Space Surveillance Workshop, April 1996.

Phan D. Dao, Patrick J. McNicholl, James H. Brown, Justin E. Cowley, Mike J. Kendra, Peter N. Crabtree, Anthony V. Dentamaro, Eileen V. Ryan, William Ryan, *Space Object Characterization with 16-Visible-Band Measurements at Magdalena Ridge Observatory*, 2008 AMOS Conference, Maui.

Anil B Chaudhary, Tamara Payne, Keith Lucas, Kimberly K.J. Kinateder, Phan Dao and Jeremy Murray-Krezan, *Propagation of Bayesian belief for near-real time statistical assessment of geosynchronous satellite status based on non-resolved photometry data*, 2014 AMOS Conference proceeding, 2014.

Payne,T. E., Gregory, S. A., Houtkooper, N. M., Burdullis, T. W.,*Analysis of Multispectral Radiometric Signatures from Geosynchronous Satellites*, Proceedings of the SPIE Astronomical Telescopes and Instrumentation – Astronomical Data Analysis II, Kona, HI, August 2002.

Fulcoly, D., et al., *Geostationary Observations with Latitudinal Diversity Simultaneously (GOLDS): Characterizing GEO Spacecraft Pose and Panels Using Photometry*, AFRL Report.

Lawrence Rabiner, *A Tutorial in Hidden Markov Models and Selected Applications in Speech Recognition*, Proceedings of the IEEE vol. 77, No. 2, 1989.

James K. Baker, *The DRAGON system—An overview*, IEEE Transactions on Acoustics, Speech, and Signal Processing , vol. 23, 24–29, 1975.

Dempster, A.P., Laird, N.M.; Rubin, D.B., *Maximum Likelihood from Incomplete Data via the EM Algorithm*, Journal of the Royal Statistical Society, Series B 39 (1): 1–38, 1977.

Y. Bengio, *Markovian Models for sequential Data*, Neural Computing Surveys, 2:129-162, 1999.

Kevin Murphy, *The Bayes Net Toolbox for Matlab*, available at and accessed on 2015-07-08: http://www.cs.ubc.ca/~murphyk/Papers/bnt.pdf.

2015 AMOSTECH Paper ID: 3278714

Biography:

Phan Dao is a Principal Research Physicist at the Air Force Research Laboratory, Space Vehicles Directorate. He graduated with a PhD degree in Physics from University of Colorado in 1985 and has been working on techniques of analyzing non-resolved photometric signatures to characterize GEO objects since 2004. He is also interested in atmospheric remote sensing and space debris assessment.